ROYAL SOCIETY OF CHEMISTRY

COMMUNICATION

Check for updates

PEA$_2$SnBr$_4$: a water-stable lead-free two-dimensional perovskite and demonstration of its use as a co-catalyst in hydrogen photogeneration and organic-dye degradation†

Lidia Romani,[a] Anu Bala, [b] Vijay Kumar, [bc] Andrea Speltini,[d] Antonella Milella,[e] Francesco Fracassi,[e] Andrea Listorti, [e] Antonella Profumo[a] and Lorenzo Malavasi [*a]

A novel lead-free 2D perovskite, namely PEA$_2$SnBr$_4$, shows impressive water-resistance by retaining its original crystal structure and optical properties when placed in contact with water. Such key properties have been advantageously used for the fabrication of a novel co-catalytic system by coupling PEA$_2$SnBr$_4$ with graphitic carbon nitride. PEA$_2$SnBr$_4$/g-C$_3$N$_4$ composites at different metal halide perovskite loadings (5 and 15 wt%) have been prepared and tested in hydrogen photogeneration in an aqueous environment and organic dye degradation (methylene blue). The results show an impressive enhancement of H$_2$ production of the composite with respect to the two separate components with hydrogen evolution rates up to 1600 μmol g^{-1} h^{-1} and analogous improvements in the efficiency of methylene blue degradation. The present results, providing a novel water-resistant perovskite and co-catalytic system, pave the way towards the safe, efficient and real use of metal halide perovskites in catalysis.

The poor water stability of tridimensional (3D) metal halide perovskites (MHPs) is a major concern, and it limits their application in solar cell technology and optoelectronic devices.[1–5] Such an issue can be overcome by using two-dimensional (2D) layered perovskites of the general formula R$_2$(CH$_3$NH$_3$)$_{n-1}$B$_n$X$_{3n+1}$, where n represents the number of inorganic layers; R represents a large organic cation, for example C$_6$H$_5$(CH$_2$)$_2$NH$_3^+$ (phenylethyl-ammonium, PEA); B represents a metal cation and X represents a halide. The improved moisture resistance of 2D perovskites comes from the presence of the hydrophobic R groups occupying the surface sites and protecting the inorganic layers from water.[1] To date, several examples of the use of 2D protecting layers in perovskite solar cells with a 2D/3D architecture have been reported.[2–10] On the other hand, the exceptional optical properties of metal halide perovskites could be used to explore their application in other fields, such as photocatalysis. In this respect, some examples of hydrogen photogeneration by metal halide perovskites have been reported in the current literature, where, due to the inherent water instability of MHPs, the use of concentrated solutions of hydracids (such as HI) was required to avoid decomposition.[11–15] We have recently shown that it is possible to achieve an improved stability of a selected 3D lead-free MHP (namely DMASnBr$_3$, DMA = dimethylammonium) in water where, possibly, the hydrophobic organic group protects the perovskite from both water and tin oxidation, as recently also found by computational modelling.[15,16] This unexpected water-stability of DMASnBr$_3$ has also been confirmed for the iodide composition.[17] In order to envisage novel applications of MHPs, in particular in the photocatalysis field, we have devised a novel 2D lead-free perovskite that could meet the pre-requisites of water stability, suitable optical properties for co-catalysis, and no environmental concerns. As will be shown below, the PEA$_2$SnBr$_4$ 2D perovskite allowed us to achieve all these goals, showing an unprecedented water stability that was exploited in the preparation of novel co-catalysts with graphitic carbon nitride (g-C$_3$N$_4$), a state-of-the-art material for visible light catalysis.[18–22]

PEA$_2$SnBr$_4$ was synthesized by a wet-chemistry route in the form of bulk material (see details in the ESI†) and its X-ray diffraction (XRD) pattern is shown in Fig. 1a (bottom part, black curve). The crystal structure agrees with the orthorhombic *Cmca* space group symmetry that we defined for the BZA$_2$SnBr$_4$ material and the pattern is dominated by (h00) reflections, a typical feature of these 2D perovskites.[23] Before preparing the final catalyst, the water stability of the perovskite was tested in two ways: (i) by dispersing the powders in distilled water under

[a] *Department of Chemistry and INSTM, University of Pavia, Via Iaramelli 12, Pavia 27100, Italy. E-mail: lorenzo.malavasi@unipv.it*

[b] *Center for Informatics, School of Natural Sciences, Shiv Nadar University, NH-91, Tehsil Dadri, Gautam Buddha Nagar, 201314, Uttar Pradesh, India*

[c] *Dr. Vijay Kumar Foundation, 1969, Sector 4, Gurgaon 122001, Harayana, India*

[d] *Department of Drug Sciences, University of Pavia, Via Taramelli 12, Pavia 27100, Italy*

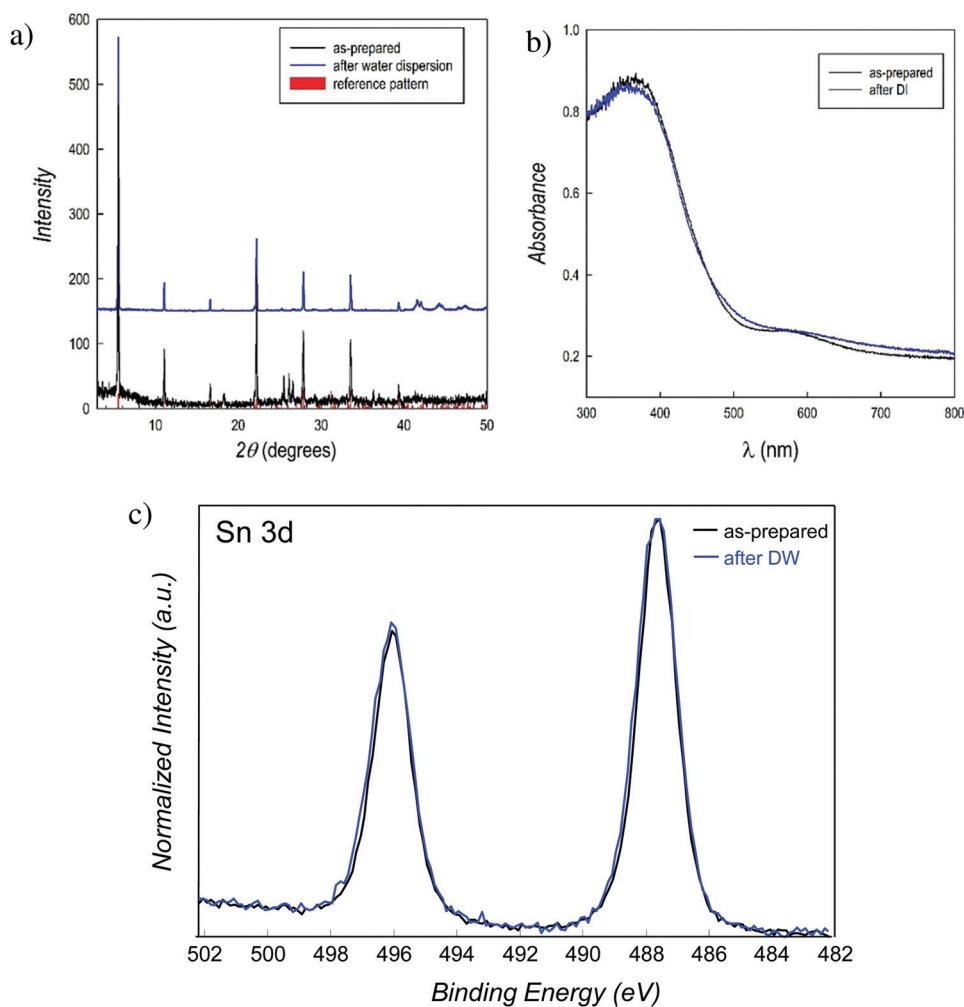[e] *Department of Chemistry, University of Bari, Via Orabona 4, Bari, 70126, Italy*

Fig. 1 (a) XRD pattern of PEA_2SnBr_4 synthesized by wet-chemistry where the red vertical bars refer to the reflection positions of the orthorhombic structure of the perovskite; bottom pattern: the as-prepared material; top pattern: after recovery from DW; (b) the UV-vis spectra of the as-prepared PEA_2SnBr_4 and after recovery from DW; (c) Sn 3d XPS spectra of the as-synthesized PEA_2SnBr_4 (black) and after recovery from aqueous solution (blue).

stirring and recovering them by filtration and (ii) by measuring the amount of tin in deionized water (DW) after perovskite removal (leaching test – see the ESI† for details). Fig. 1a (top pattern, blue curve) shows the XRD pattern of PEA_2SnBr_4 after 4 hours in DW under stirring, which is superimposable onto that of the starting material, thus confirming that this perovskite does not dissolve in water (also, by visual inspection, it is possible to note the presence of particles in the water). A further comparison of the two patterns is shown in the ESI† as the square root of the intensity, in order to possibly put in prominence a very low amount of impurities (Fig. S1, ESI†). Moreover, the leaching test showed that just 0.14 wt% of the initial amount of tin in the perovskite is released in water after 4 h stirring (see the ESI†), confirming the exceptional water-stability of this material. The UV-vis absorbance spectra of the perovskite before (as-prepared) and after water dispersion are shown in Fig. 1b and again the absorption edge remains fixed at 2.67 eV without the appearance of any absorption tail. The defect state associated with Sn^{2+} to Sn^{4+} oxidation is well known to cause a significant change in the optical properties of the

MHPs.[24] Finally, the strongest proof of water stability comes from the results of X-ray photoelectron spectroscopy (XPS) analysis. Fig. 1c shows the Sn 3d XPS spectra of the as-prepared PEA_2SnBr_4 and that after 4 hours in DW under stirring. The binding energies correspond to those of Sn^{2+} (487.6 eV), and as can be seen, the two spectra are superimposable both in terms of the position and shape, confirming the extraordinary water-stability of PEA_2SnBr_4 and the absence of any oxidation.[25] We remark that a very recent computational modeling work indicated that the presence of PEA hydrophobic groups not only protects the inorganic layer from water but also protects tin from oxidation.[16] It may be possible that the presence of long and hydrophobic organic groups directly linked to the single inorganic slab creates a close and water-repellant environment that protects it both from moisture and in turn from oxidation.

After having assessed the optimal and unprecedented water-stability of PEA_2SnBr_4, we prepared composite catalytic systems by coupling this 2D lead-free perovskite, as a co-catalyst, to g-C_3N_4. This strategy is commonly used to improve the properties of C_3N_4, in particular to increase charge migration and the

9190 | *J. Mater. Chem. C*, 2020, **8**, 9189–9194

This journal is © The Royal Society of Chemistry 2020

recombination time, and to extend the absorption range.[20,21] Common composites are based on the coupling of g-C$_3$N$_4$ with metals, bimetals, semiconductors (oxides, sulfides, and the like), graphene, carbon dots, conductive polymers, and sensitizers, among others. In this respect, the unique optical properties of MHPs suggest that they can be very good candidates as co-catalysts. In addition, the band-gap of PEA$_2$SnBr$_4$ (around 2.67 eV) matches well with that of g-C$_3$N$_4$ (2.76 eV), thus suggesting a possible synergic effect between the two materials.

PEA$_2$SnBr$_4$/g-C$_3$N$_4$ composites at different MHP loadings (5 and 15 wt%) were synthesized by a wet-chemistry route (see the ESI†) and their crystal structures were characterized by using X-ray diffraction (Fig. S2, ESI†). The composites reveal an overall amorphous-like structure, with the main peak of g-C$_3$N$_4$ (around 27.5°) and the general sample scattering becoming progressively less intense with the increasing amount of metal halide perovskite. No clear diffraction peaks of crystalline perovskites were found in the patterns, suggesting that this can be due the presence of g-C$_3$N$_4$ during perovskite synthesis which tends to reduce the structural order of PEA$_2$SnBr$_4$, and/or to the formation of small perovskite particles on carbon nitride, as revealed by the significant change of morphology passing from pristine g-C$_3$N$_4$ to the composite (Fig. S3, ESI†). Energy dispersive X-ray (EDX) analysis of the composites confirmed the homogenous distribution of metal and halide, and the expected Sn/Br ratio, ruling out the formation of different phases and/or clusters (Table S1, ESI†). The XPS spectra of N 1s confirmed the presence of quaternary ammonium around 401.4 eV in both composites, which is absent in pristine carbon nitride (Fig. S4, ESI†).[26,27] Also, the Sn 3d XPS spectra of both composites (Fig. S5, ESI†) show analogous signals to the starting PEA$_2$SnBr$_4$ with a slight shift to lower binding-energies (less than 1 eV), which rules out any oxidation during composite preparation (Sn^{4+} would appear at higher binding energies than Sn^{2+}). The origin of this shift goes beyond the scope of the present paper, and may be related to the interaction between the perovskite and g-C$_3$N$_4$ as well as to the peculiar morphology of the composites and will be the subject of future work.

The optical absorbance spectra of the PEA$_2$SnBr$_4$/g-C$_3$N$_4$ composites (Fig. 2a) show the expected predominance of the g-C$_3$N$_4$ feature for both 5 and 15% perovskite loadings, by keeping the absorbance threshold around 2.76 eV (see the Tauc plots in the ESI,† Fig. S6). This result could also be anticipated considering the relatively small difference in the band gap between carbon nitride and PEA$_2$SnBr$_4$.

Once the pure perovskite and the composites were characterized, we focused on the evaluation of their photocatalytic properties, by looking at hydrogen photogeneration from water and the degradation of model organic water pollutants, by employing common protocols used for similar g-C$_3$N$_4$-based composites.[22] The results reported in the following have been obtained on several replicas of the composites and the experimental details of the hydrogen evolution tests are reported in the Experimental Section (ESI†).

Firstly, the hydrogen photogeneration efficiency of the PEA$_2$SnBr$_4$/g-C$_3$N$_4$ composites (5 and 15 wt% of perovskites

with respect to g-C$_3$N$_4$) has been determined in water containing 10% triethanolamine (TEOA), as a typical sacrificial agent, and with a 3 wt% Pt loading. We stress that these are the conditions used to test all carbon nitride-based materials, as can be inferred from ref. 14–18. The H$_2$ evolution rates (HERs) as a function of perovskite loading of the composites are reported in Table 1.

From the data reported in Table 1, it is possible to make several conclusions: (i) hydrogen production (4 µmol g^{-1} h^{-1}) is achieved by the perovskite alone; (ii) g-C$_3$N$_4$ shows a significant HER of 81 µmoles g^{-1} h^{-1}; (iii) an impressive synergic effect is observed for both composites, providing HERs that are more than 20 and 10 times that of pure carbon nitride for the perovskite loading of 5 and 15%, respectively; (iv) comparing the data of pure g-C$_3$N$_4$ and that of the two composites, it is possible to suggest an optimal loading of PEA$_2$SnBr$_4$ of around 5 wt%. Finally, a HER of about 1600 µmol g^{-1} h^{-1} for the PEA$_2$SnBr$_4$/g-C$_3$N$_4$ composite with 5% perovskite places it close to that of materials with an ultra-high HER.[22] Table 1 also reports the effectiveness of PEA$_2$SnBr$_4$/g-C$_3$N$_4$ (5 wt% perovskite – the best performing composite) for photogeneration activity in 0.1 M aqueous glucose, a representative of a biomass-derived sacrificial agent. The HER for the composite was 107 µmol g^{-1} h^{-1} and that of pure g-C$_3$N$_4$ was 3 µmol g^{-1} h^{-1}, *i.e.* a 30-fold improvement. To check the stability of the PEA$_2$SnBr$_4$/g-C$_3$N$_4$ composites after the photogeneration reaction, the reaction solution was filtered and the powder was recovered and subjected to XRD and UV-vis spectroscopy analyses. The patterns of the composites before and after the photocatalytic tests are shown in Fig. 2b and c, showing unaltered patterns of the spent catalysts compared to those of the starting material. No evidence of reduction products (*e.g.* elemental tin) was found in the patterns, confirming the stability of the composites. Moreover, compared to the as-prepared powder, the UV-vis spectra also remain unchanged for the spent catalyst (Fig. 2d for 5 wt%, as the selected example). Finally, EDX analysis confirmed the preservation of the Sn/Br ratio of the 2D perovskite in the composite.

The composite with a higher HER was also tested to check its activity towards the decomposition of organic dyes, by selecting methylene blue (MB) as a representative model compound of this class. Fig. 3 shows the variation of MB concentration (plotted as C/C_0, where C_0 is the initial concentration) as a function of irradiation time, compared to that of pure g-C$_3$N$_4$ and direct photolysis (see details in the ESI†).

It is clear from Fig. 3, as for the hydrogen photogeneration, that the reported novel composite also performs better than pure carbon nitride with respect to organic dye degradation. In particular, pristine g-C$_3$N$_4$ cannot completely degrade MB even after 90 minutes of irradiation, while the PEA$_2$SnBr$_4$/g-C$_3$N$_4$ composite completely decomposes the dye in about 40 minutes.

The particularly efficient performance of the PEA$_2$SnBr$_4$/g-C$_3$N$_4$ composite can be understood on the basis of the relative band-alignment of the two semiconductors when present in the composite.
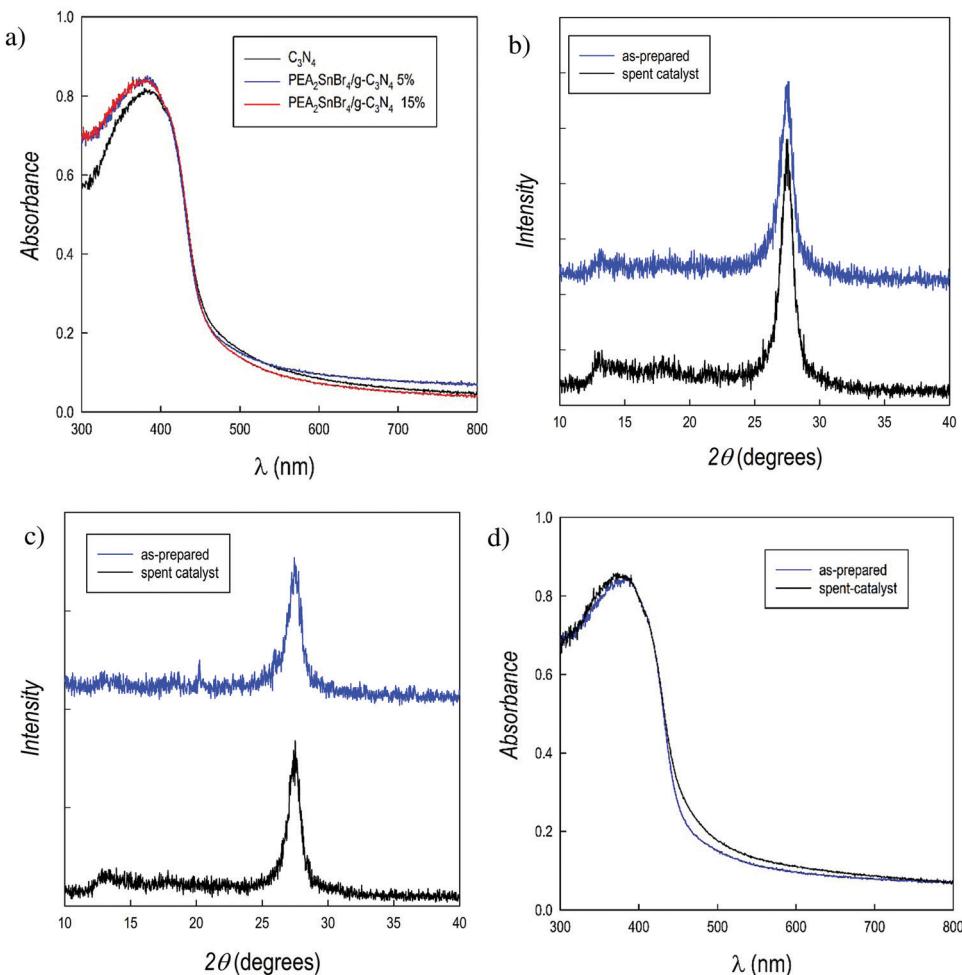
This journal is © The Royal Society of Chemistry 2020

J. Mater. Chem. C, 2020, **8**, 9189–9194 | **9191**

Fig. 2 (a) UV-vis spectra of pristine g-C$_3$N$_4$ and PEA$_2$SnBr$_4$/g-C$_3$N$_4$ composites; (b) XRD pattern of PEA$_2$SnBr$_4$/g-C$_3$N$_4$ 5% composite as-prepared and after the H$_2$ photogeneration experiment (spent catalyst); (c) XRD pattern of PEA$_2$SnBr$_4$/g-C$_3$N$_4$ 15% composite as-prepared and after the H$_2$ photogeneration experiment (spent catalyst); (d) UV-vis spectra of PEA$_2$SnBr$_4$/g-C$_3$N$_4$ 5% composite as-prepared and after the H$_2$ photogeneration experiment (spent catalyst).

Table 1 Hydrogen Evolution Rates (HERs) from aqueous solutions for g-C$_3$N$_4$ and PEA$_2$SnBr$_4$/g-C$_3$N$_4$ composites at different percentages of MHP loadings as well as for PEA$_2$SnBr$_4$ (1 g L^{-1} catalyst, 3 wt% Pt, 6 h irradiation under simulated solar light, 500 W m^{-2}). The standard deviation is shown in parentheses (RSD $\leq$ 10%, n = 3)

	HER (μmoles g^{-1} h^{-1})	
	10% TEOA	0.1 M glucose
PEA$_2$SnBr$_4$	4(0.4)	<0.1
PEA$_2$SnBr$_4$/g-C$_3$N$_4$ 5%	1613(98)	107(8)
PEA$_2$SnBr$_4$/g-C$_3$N$_4$ 15%	963(59)	n.d.
g-C$_3$N$_4$	81(6)	3(0.3)

n.d., not determined.

The valence band maximum (VBM) and conduction band minimum (CBM) edge positions of g-C$_3$N$_4$ and PEA$_2$SnBr$_4$ relative to the NHE potential were calculated using the work function method:

$$E_{\mathrm{VBM}} = -\Phi - 0.5E_{\mathrm{g}}$$

$$E_{\mathrm{CBM}} = -\Phi + 0.5E_{\mathrm{g}}$$

$$E_{\mathrm{CBM(VBM)}}' = -E_{\mathrm{CBM(VBM)}} - 4.5$$

where Φ is the work function defined as the minimum energy required to extract an electron from a material, and is equal to the energy difference between the Fermi level and the electrostatic potential energy in a vacuum. Further, E_{g} is the band gap and $E_{\mathrm{CBM(VBM)}}'$ is the potential $vs.$ NHE, and they are reported in Fig. 4.[28,29] The calculated Φ values of g-C$_3$N$_4$ (the optimized structure, see Fig. S7, ESI†) and PEA$_2$SnBr$_4$ (the optimized structure, see Fig. S8, ESI†) obtained using the HSE06 functional are 4.61 eV (Fig. S9, ESI†) and 4.14 eV (Fig. S10, ESI†), respectively. Notably, the calculated E_{g} values with HSE06 for the g-C$_3$N$_4$ (2.8 eV) and PEA$_2$SnBr$_4$ (2.74 eV) monolayers are in good agreement with the experimental values of 2.76 eV and 2.67 eV, respectively. As depicted in Fig. 4, the CBMs of g-C$_3$N$_4$ and PEA$_2$SnBr$_4$ are located at −1.29 V and −1.74 V $vs.$ NHE, which are above the H$^+$/H$_2$ potential, whereas the VBM of

9192 | J. Mater. Chem. C, 2020, 8, 9189–9194

This journal is © The Royal Society of Chemistry 2020

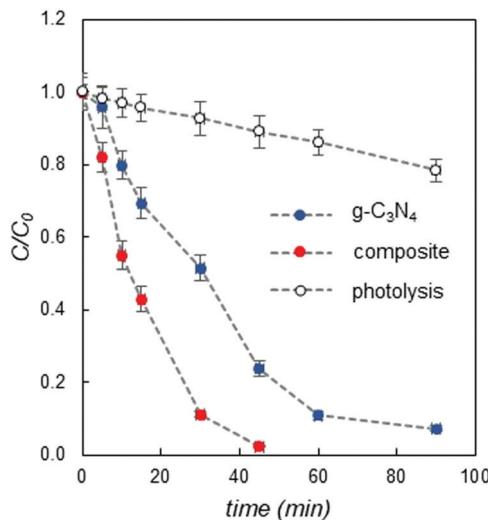**Fig. 3** Variation of MB concentration as a function of irradiation time for g-C_3N_4 (blue dots) and the PEA_2SnBr_4/g-C_3N_4 5% composite (red dots), compared to the photolysis effect (empty dots); conditions: 1 g L^{-1} catalyst, 250 W m^{-2} simulated solar light. RSD < 10% (n = 3).
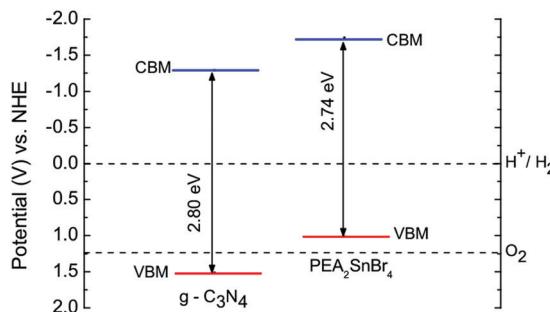

Fig. 4 Calculated band edge positions (solid lines) for two semiconductors relative to NHE potential. The two dashed lines indicate the water redox reaction potentials.

g-C_3N_4 is at 1.51 V *vs.* NHE, below the O_2 potential. Since the band gap values of both semiconductors are comparable, electron–hole pairs are generated in both the semiconductors under visible-light irradiation. As a consequence of the band alignment shown in Fig. 4, the photo-induced electrons from PEA_2SnBr_4 can easily move towards g-C_3N_4 due to the CBM lying at a less negative potential. Finally, the accumulated electrons take part in the photochemical reduction of water to generate hydrogen. In this way, the hetero-junction formed could limit the recombination rate of the photo generated electron–hole pairs, thus remarkably increasing the photo-catalytic activity for hydrogen evolution compared to that of pure g-C_3N_4.

Conclusion

A novel 2D lead-free metal halide perovskite, PEA_2SnBr_4, has been synthesized and characterized, showing an impressive and unprecedented water-resistance in both structural and optical properties. Such features have been exploited in the preparation of novel co-catalytic systems by coupling PEA_2SnBr_4 with g-C_3N_4 due to the close band-gap of the two semiconductors. The composites synthesized showed an impressive synergic effect in the enhancement of photocatalytic hydrogen production in an aqueous environment as well as in the degradation of organic dyes, without any degradation observed in the spent catalyst. Computational modelling provides a description of the favorable band-alignment between PEA_2SnBr_4 and g-C_3N_4, thus confirming the synergic role from a microscopic point of view. The discovery of this water-stable metal halide perovskite allows us to explore new applications of these materials, taking advantage of their superior optical properties in catalysis under experimental conditions, which has not been possible to date.

Conflicts of interest

There are no conflicts to declare.

Acknowledgements

References

1 P. Gao, A. R. B. M. Yusoff and M. K. Nazeeruddin, *Nat. Commun.*, 2018, **9**, 5028.
2 H. Xu, Y. Sun, H. Zheng, G. Liu, X. Xu, S. Xu, L. Zhang, X. Chen and X. Pan, *J. Mater. Chem. C*, 2019, **7**, 15276–15284.
3 J. Schlipf, Y. Hu, S. Pratap, L. Biessmann, N. Hohn, L. Porcar, T. Bein, P. Docampo and P. Muller-Buschbaum, *ACS Appl. Energy Mater.*, 2019, **2**, 1011–1018.
4 I. C. Smith, E. T. Hoke, D. Solis-Ibarra, M. D. McGehee and H. I. A. Karunadasa, *Angew. Chem.*, 2014, **126**, 11414–11417.
5 Y. Hu, T. Qiu, F. Bai, W. Ruan and S. Zhang, *Adv. Energy Mater.*, 2018, **8**, 1703620.
6 A. Z. Chen, M. Shiu, J. H. Ma, M. R. Alpert, D. Zhang, B. J. Foley, D.-M. Smilgies, S.-H. Lee and J. J. Choi, *Nat. Commun.*, 2018, **9**, 1336.
7 D. H. Cao, C. C. Stoumpos, O. K. Farha, J. T. Hupp and M. G. Kanatzidis, *J. Am. Chem. Soc.*, 2015, **137**, 24.
8 H. Tsai, W. Nie, J.-C. Blancon, C. C. Stoumpos, R. Asadpour, B. Harutyunyan, A. J. Neukirch, R. Verduzco, J. J. Crochet, S. Tretiak, L. Pedesseau, J. Even, M. A. Alam, G. Gupta, J. Lou, P. M. Ajayan, M. J. Bedzyk, M. G. Kanatzidis and A. D. Mohite, *Nature*, 2016, **536**, 312–316.
9 L. N. Quan, M. Yuan, R. Comin, O. Voznyy, E. M. Beauregard, S. Hoogland, A. Bunin, A. R. Kirmani, K. Zhao, A. Amassian, D. H. Kim and E. H. Sargent, *J. Am. Chem. Soc.*, 2016, **138**, 2649–2655.

This journal is © The Royal Society of Chemistry 2020

J. Mater. Chem. C, 2020, **8**, 9189–9194 | **9193**

10 T. Ming Koh, V. Shanmugam, X. Guo, S. S. Lim, O. Filonik, E. M. Herzig, P. Mueller-Buschbaum, V. Swamy, S. T. Chien, S. G. Mhaisalkar and N. Mathews, *J. Mater. Chem. A*, 2018, **6**, 2122–2128.

11 Z. Zhao, J. Wu, Y.-Z. Zheng, N. Li, X. Li and X. Tao, *ACS Catal.*, 2019, **9**, 8144–8152.

12 S. Park, W. J. Chang, C. W. Lee, S. Park, H.-Y. Ahn and K. T. Nam, *Nat. Energy*, 2016, **2**, 16185.

13 M. Wang, Y. Zuo, J. Wang, Y. Wang, X. Shen, B. Qiu, L. Cai, F. Zhou, S. P. Lau and Y. Chai, *Adv. Energy Mater.*, 2019, **9**, 1901801.

14 Z. Zhao, J. Wu, Y.-Z. Zheng, N. Li, X. Li, Z. Ye, S. Lu, X. Tao and C. Chen, *Appl. Catal., B*, 2019, **253**, 41–48.

15 A. Pisanu, A. Speltini, P. Quadrelli, G. Drera, L. Sangaletti and L. Malavasi, *J. Mater. Chem. C*, 2019, **7**, 7020.

16 A. Bala and V. Kumar, *J. Phys. Chem. C*, 2019, **123**, 25176–25184.

17 D. Ju, X. Zheng, J. Liu, Y. Chen, J. Zhang, B. Cao, H. Xiao, F. O. Mohammed, O. M. Bakr and X. Tao, *Angew. Chem., Int. Ed.*, 2018, **57**, 14868–14872.

18 S. Cao, J. Low, J. Yu and M. Jaroniec, *Adv. Mater.*, 2015, **27**, 2150–2176.

19 S. Ye, R. Wang, M.-Z. Wu and Y.-P. Yuan, *Appl. Surf. Sci.*, 2015, **358**, 15–27.

20 Z. Zhao, Y. Sun and F. Dong, *Nanoscale*, 2015, **7**, 15.

21 N. Fajrina and M. A. Tahir, *Int. J. Hydrogen Energy*, 2019, **44**, 540–577.

22 G. Liao, Y. Gong, L. Zhang, H. Gao, G.-J. Yang and B. Fang, *Energy Environ. Sci.*, 2015, **7**, 15.

23 A. Pisanu, M. Coduri, M. Morana, Y. O. Ciftci, A. Rizzo, A. Listorti, M. Gaboardi, L. Bindi, V. I. E. Queloz, C. Milanese, G. Grancini and L. Malavasi, *J. Mater. Chem. A*, 2020, **8**, 1875–1886.

24 T. B. Song, T. Yokoyama, C. C. Stoumpos, J. Logsdon, D. H. Cao, M. R. Wasielewski, S. Aramaki and M. G. Kanatzidis, *J. Am. Chem. Soc.*, 2017, **139**, 836–842.

25 L. Hou, Y. Zhu, J. Zhu and C. Li, Tuning Optical Properties of Lead-Free 2D Tin-Based Perovskites with Carbon Chain Spacers, *J. Phys. Chem. C*, 2019, **123**, 31279.

26 Z.-A. Lan, G. Zhang and X. Wang, A facile synthesis of Br-modified g-C_3N_4 semiconductors for photoredox water splitting, *Appl. Catal., B*, 2016, **192**, 116.

27 G. Beamson and D. Briggs, *High Resolution XPS of Organic Polymers – The Scienta ESCA300 Database*, Wiley Interscience, 1992, p. 278.

28 O. Francis, K. G. Krishna, G. C. E. Cornelia and P. G. Penny, *Appl. Surf. Sci.*, 2018, **427**, 487–498.

29 K. K. Dalal and A. C. Emily, *J. Phys. Chem. C*, 2012, **116**, 9876–9887.